01 Jan 2023

A Deep Learning-Informed Design Scheme For Shear Friction At Concrete-to-Concrete Interface: Recommendations For Inclusion In AASHTO LRFD Guidelines

Tarutal Ghosh Mondal

Nikkolas Edgmond

Lesley Sneed
Missouri University of Science and Technology, sneedlh@mst.edu

Genda Chen
Missouri University of Science and Technology, gchen@mst.edu

TRR
JOURNAL OF THE TRANSPORTATION RESEARCH BOARD

Research Article

Transportation Research Record
1–9

DOI: 10.1177/03611981231183718
journals.sagepub.com/home/trr
Sage

A Deep Learning-Informed Design Scheme for Shear Friction at Concrete-to-Concrete Interface: Recommendations for Inclusion in AASHTO LRFD Guidelines

Tarutal Ghosh Mondal[1], Nikkolas Edgmond[2,3], Lesley Sneed[4], and Genda Chen[1]

Abstract

Recent advancements in construction technology have led to high-strength concrete and steel. However, these developments have depreciated the accuracy of the design equations in current provisions, which were based on normal-grade materials. To fill such a research gap, this study presents a novel deep learning-based computation scheme that can replace the current design provisions by virtue of its superior accuracy and reliability. The proposed approach exploits Neural Additive Models (NAMs) in which geometric and material properties associated with a normalweight concrete-to-concrete shear interface are inputted to individual neural network blocks. The outputs of the individual blocks are linearly combined to produce the prediction for interfacial shear strength. This model provides a way to identify and quantify the individual contributions of the input parameters, thus enhancing the interpretability of the model predictions for shear strength at the normalweight concrete-to-concrete interface. The deep learning-informed design (LID) scheme improves the prediction accuracy of the shear strength equation in the existing AASHTO LRFD Bridge Design Specifications by over 32%.

Keywords

learning-informed design, neural additive models, interfacial shear strength, concrete-to-concrete interface, shear friction

Structural engineers rely heavily on code and specification equations (*1*, *2*) for the design of various structural components. In many cases, these design provisions were developed decades ago based on the results of laboratory experiments. Over the years, the strength of many construction materials (e.g., concrete and steel) has improved considerably (*3*, *4*). This has, to a certain extent, outdated the experimental results on which the design equations were based. The current design provisions limit the allowable material strength as a way to keep the design within the parameters of the empirical formulas. As a result, the current provisions fail to live up to the expectations of accurate and economical design, indicating an urgent need for modifications (*5*). On the other hand, recent advances in artificial intelligence (AI) have provided an unprecedented opportunity of modeling complex nonlinear relations in an accurate and efficient way (*6*).

Although AI has been around for quite some time, its application in accurately predicting various design

[1]Department of Civil, Architectural and Environmental Engineering, Center for Intelligent Infrastructure (CII), INSPIRE University Transportation Center, Missouri University of Science and Technology, Rolla, MO
[2]Department of Civil, Architectural and Environmental Engineering, Missouri University of Science and Technology, Rolla, MO
[3]Genesis Structures Inc, Kansas City, MO
[4]Department of Civil, Materials, and Environmental Engineering, University of Illinois Chicago, IL

Corresponding Author:
Genda Chen, gchen@mst.edu

parameters has not received adequate attention from the scientific community (*7*). A few studies explored deep learning techniques for predicting the compressive strength (*8*, *9*), shear strength (*10*, *11*), and elastic modulus (*12*) of concrete. However, it has not been used to predict the interfacial shear strength of normalweight concrete-to-concrete interfaces. The present study aims to fill this knowledge gap by proposing a generalized framework for developing an interpretable learning-informed design (LID) scheme, which may replace some of the design equations in the current codes and specifications in the future. The proposed design scheme is based on Neural Additive Models (NAMs) that combine the expressivity of deep neural networks with the inherent intelligibility of generalized additive models. NAMs learn a linear combination of neural networks, each attending to a single input feature. The networks are trained jointly and can learn arbitrarily complex relationships between the response and predictor variables. Each trained subnet can be represented as a graph quantifying the contribution of respective features to the final output. This affords interpretability to the design scheme, providing an insight into how model outputs are generated. NAMs have been used in the past for various applications such as nowcasting (*13*), financial decision-making (*14*), and survival analysis (*15*), apart from the prediction of heart attack, housing price, recidivism risk, critical temperature of superconductors, and personalized treatment benefits for Covid-19 patients (*16–18*). However, this approach has never been used to predict the mechanical properties of structural materials, which is the scope of this study.

This study presents a novel deep learning-based computation scheme for predicting the design parameters of structural design provisions. The prediction of shear strength at the normalweight concrete-to-concrete interface is used as a case study to demonstrate the feasibility of this approach based on the test data collected from the literature (*5*). With appropriate modifications, the LID scheme can be extended to other applications such as the estimation of the residual strength of corroded steel members, the fatigue resistance of welded steel connections, and the capacity of different types of piles in soil.

The Proposed Method

A generalized framework is proposed for developing a LID scheme based on recent development in the area of deep learning called NAMs (*12*). This modeling approach is based on a neural network that comprises several subnetworks, each attending to a single input parameter (Figure 1). The outputs of the independent subnetworks, represented by shape functions $f_i(\bar{x}_i)$ $(i = 1, 2, \ldots, n)$, are linearly combined to produce the final network output y (Equation 1). The work presented here utilized a simple linear combination of shape functions. However, future studies should investigate other strategies that may improve the prediction accuracy.

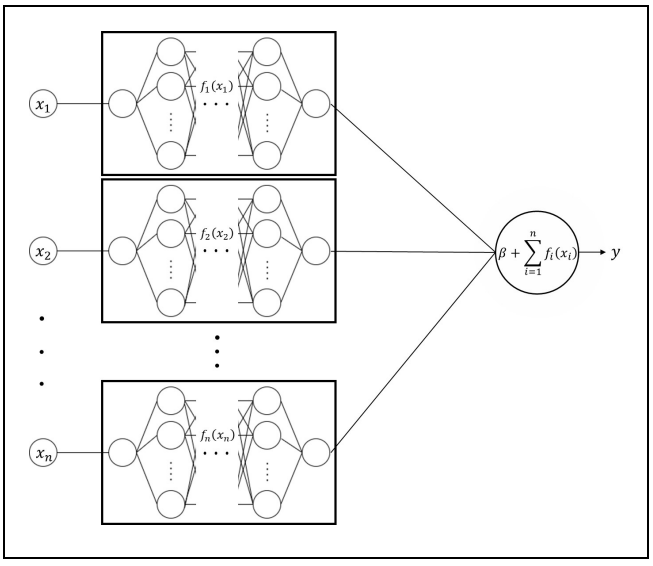

Figure 1. Neural additive models.

$$y = \beta + f_1(\bar{x}_1) + f_2(\bar{x}_2) + \cdots\cdots + f_n(\bar{x}_n) \quad (1)$$

where $\bar{x}_1, \bar{x}_2, \cdots\cdots, \bar{x}_n$ are normalized parameters given by

$$\bar{x}_i = \frac{x_i - x_{i,min}}{x_{i,max} - x_{i,min}} \quad (2)$$

$x_{i,min}$ and $x_{i,max}$ are the minimum and maximum values for the i^{th} input parameter, respectively, and β is the bias term. Once the training is complete, the contribution of each parameter to the final output can be plotted against the normalized parameter values, giving rise to shape functions that can also be presented in a tabular format. At test time, the shape function values can be estimated for a set of known normalized parameters and added as per Equation 1 to produce the final model prediction. This makes the decision-making far more interpretable, as the contribution of each input parameter can be evaluated on an individual basis. It can be mentioned in this context that the traditional neural network techniques are not fully embraced by the structural engineering community because of the inherent computational complexity and the lack of interpretability. However, the shape functions generated by the NAMs make the neural network redundant, as these shape functions are all it needs to compute the nominal shear strength of a concrete-to-concrete interface. This results in a new design paradigm that is generated by a neural network but does not

Table 1. Cohesion and Friction Factors for Normalweight Concrete Interfaces as Prescribed by AASHTO LRFD Bridge Design Specifications (*1*); for Brackets, Corbels, and Ledges, *c* is set to zero

Description	*c* (MPa)	μ	K_1	K_2 (MPa)
Concrete placed monolithically	2.8	1.4	0.25	10.3
Concrete placed against a clean concrete surface, free of laitance with surface roughened to an amplitude of 6 mm	1.9	1.0	0.3	12.4
Concrete placed against a clean concrete surface, free of laitance, but not intentionally roughened	0.52	0.6	0.2	5.5

explicitly involve one in its final computational scheme, thanks to the unique capabilities of NAMs.

Case Study: Prediction of Shear Strength at Concrete-To-Concrete Interface

Transfer of direct shear across a concrete-to-concrete interface is a common phenomenon in reinforced concrete (RC) structures containing an existing crack or interface between concrete cast at different times. The safe and efficient design of such interfaces is important as there is little or no load-path redundancy. This calls for an accurate prediction of the interfacial shear strength, which current design specifications like AASHTO LRFD (*1*) aim to facilitate through a set of decades-old empirical relations as shown in Equation 3:

$$v_n = c + \mu\left(\rho f_y + \sigma_N\right) \tag{3}$$

where v_n is the nominal interfacial shear stress given by the shear strength divided by the area of the interface; c is the cohesion factor that is set to zero for brackets, corbels, and ledges, as the effectiveness of cohesion and aggregate interlock is unreliable along a vertical crack interface; ρ is the shear reinforcement ratio given by the area of reinforcement crossing the interface divided by the area of the interface; f_y is the yield strength of shear reinforcement, which is not to exceed 420 MPa; μ is the friction coefficient characterizing the shear interface; and σ_N is the compressive normal stress applied to the shear interface. In the case of net tension, a part of the reinforcement crossing the interface is utilized in resisting tension and makes no contribution to the shear strength. The remaining reinforcement is used to compute the nominal shear stress as per Equation 3 considering σ_N to be zero. It is to be noted here that the AASHTO LRFD Bridge Design Specifications do not specify how to deal with inclined reinforcements. However, the relation presented in Equation 3 can be extended based on a physical model prescribed by the ACI 318 Code (*2*) for interfaces with inclined shear reinforcement as shown in Equation 4:

$$v_n = c + \rho f_y(\mu \sin\alpha + \cos\alpha) + \mu\sigma_N \tag{4}$$

in which α ($\leqslant 90°$) is the acute angle that shear reinforcement makes relative to the shear plane. The AASHTO LRFD Bridge Design Specifications limit the maximum nominal interfacial shear stress to

$$v_{n,max} = min\left\{K_1 f_c^{'}, K_2\right\} \tag{5}$$

where K_1 and K_2 are friction factors as enumerated in Table 1. $f_c^{'}$ is the compressive strength of concrete. If the concretes on the two sides of the shear interface have different strengths, the lesser value of $f_c^{'}$ should be considered.

However, these equations were derived in test conditions that may not be applicable for certain modern designs. Specifically, modern technologies have raised the strength of concrete and steel to levels well beyond those available decades ago, calling into question the applicability of the equations for these materials (*5*). This brings to the fore an urgent need to update these equations to ensure the safe and economical design of RC structures. To this end, this study proposes a novel deep learning-based approach leveraging the latest developments in NAMs to predict the interfacial shear strength at the normalweight concrete-to-concrete interface.

Learning-Informed Design Scheme

A deep learning-based computation scheme, called LID, is developed for various design parameters by leveraging the NAMs approach. The shear friction database generated by Edgmond and Sneed (*5*) was exploited in this study to train and evaluate the deep learning model. The original database comprised normalweight and lightweight concrete specimens. However, as the first step of applying the NAMs approach in civil engineering, this study is limited to normalweight concrete only, as test data on lightweight concrete are limited. The database also contained several specimens that were tested under combined shear and bending, and composite concrete beams tested under three- and four-point bending configurations for horizontal shear transfer. These specimens were removed from the database used in this study. Additionally, a few cases involved specimens with

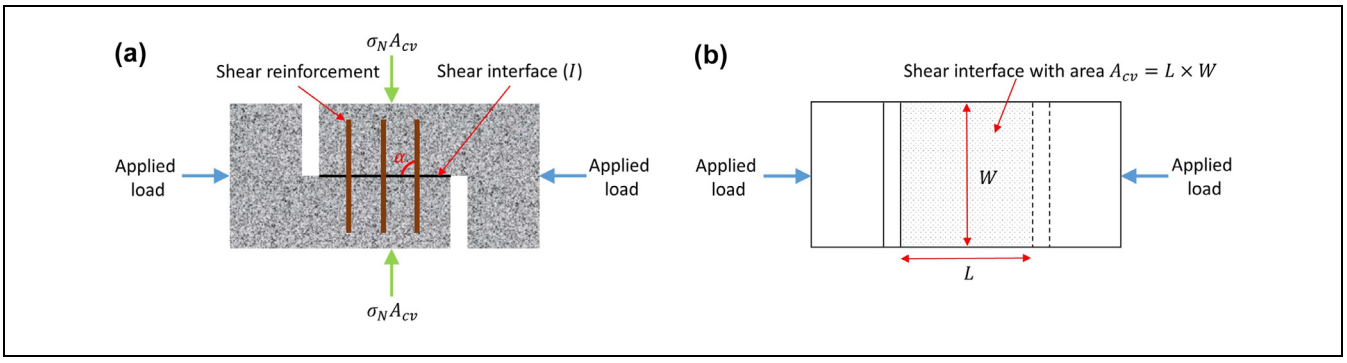

Figure 2. An illustrative sketch of a typical shear friction test. (*a*) Side view and (*b*) plan view.

Table 2. Part of the Dataset along with the Minimum and Maximum Values of the Input Parameters

Specimen	x_1	x_2 (mm)	x_3 (mm)	x_4 ($\sqrt{\text{MPa}}$)	x_5 (MPa)	x_6 (°)	x_7 (MPa)	v_n (MPa)
1	2.00	753.00	151.00	3.92	0.00	0.00	0.00	1.12
2	3.00	406.40	152.40	4.77	3.39	90.00	0.00	4.24
3	2.00	304.80	203.20	4.84	1.33	90.00	0.00	3.14
4	3.00	152.40	203.20	4.92	2.82	90.00	0.00	1.48
5	2.00	406.40	254.00	6.07	3.12	90.00	0.00	4.93
6	3.00	279.40	114.30	5.55	6.11	90.00	0.00	4.56
7	2.00	914.40	254.00	4.59	1.02	90.00	0.00	2.62
8	1.00	300.00	120.00	6.01	0.00	0.00	4.96	5.07
9	2.00	753.00	155.00	4.54	0.00	0.00	0.00	1.50
10	3.00	304.80	203.20	4.90	1.41	90.00	0.00	0.76
…	…	…	…	…	…	…	…	…
Minimum	1.00	152.40	100.00	3.86	0.00	0.00	−2.76	0.00
Maximum	3.00	914.40	610.00	10.67	15.18	135.00	10.34	18.39

inclined interfaces. These specimens were also excluded from this study. The resulting dataset contained 639 samples. The existing knowledge about the frictional response of the concrete-to-concrete interface was invoked to identify seven key parameters as described in the following equations:

$$x_1 = I \tag{6}$$

$$x_2 = L \tag{7}$$

$$x_3 = W \tag{8}$$

$$x_4 = \sqrt{min(f_{c1}, f_{c2})} \tag{9}$$

$$x_5 = \rho f_y = \frac{A_{vf}}{A_{cv}} f_y \tag{10}$$

$$x_6 = \alpha \tag{11}$$

$$x_7 = \sigma_N \tag{12}$$

where I is an integer that represents the interface type (Figure 2), which takes 1, 2, and 3 for monolithic, nonmonolithic rough, and nonmonlithic smooth surfaces, respectively; L and W are the length and width of the shear plane, respectively; f_{c1} and f_{c2} are the compressive strengths of concrete on two sides of the shear interface; A_{vf} is the area of shear reinforcement crossing the shear interface; and A_{cv} is the gross area of the shear interface. The minimum and maximum values for different parameters are shown in Table 2.

The NAMs contained seven subnetworks corresponding to seven input parameters. The subnetworks were constituted by multilayer perceptrons comprising an input layer, an output layer, and three intermediate hidden layers containing sixteen neurons each. The optimum network parameters were obtained by minimizing the mean squared error between the target and predicted interfacial shear strengths using an Adam optimizer (*19*). In this study, ten-fold cross-validation was conducted to test the generalization ability of the network. Ten percent of the available data (64) were randomly selected and set aside as the test dataset. The remaining 90% of the data (575) were used for cross-validation. Each round of cross-validation involved training the network with 90% of the cross-validation data (517) and validating with the remaining 10% (58). A large validation set will reduce the size of training data leading to overfitting. On the

Table 3. Cross-validation and Test Accuracies of the NAMs as Compared with AASHTO Calculations

	AASHTO			NAMs		
Metric	Train	Val	Test	Train	Val	Test
R^2	0.62 ($\pm$ 0.01)	0.60 ($\pm$ 0.08)	0.60	0.82 ($\pm$ 0.01)	0.82 ($\pm$ 0.03)	0.77
MAE	1.54 ($\pm$ 0.03)	1.57 ($\pm$ 0.25)	1.59	1.00 ($\pm$ 0.04)	1.04 ($\pm$ 0.09)	1.12
RMSE	2.18 ($\pm$ 0.04)	2.22 ($\pm$ 0.37)	2.28	1.48 ($\pm$ 0.04)	1.49 ($\pm$ 0.12)	1.71

Note: NAMs = Neural Additive Models; Val = validation; R^2 = coefficient of determination; MAE = mean absolute error; RMSE = root mean squared error.

other hand, a small validation dataset will be inadequate for measuring the generalizability of the network. Therefore, as a tradeoff, the percentage of the validation dataset is set at 10% in this study to strike a balance between model accuracy and generalizability.

Results and Discussion

The performance of the proposed deep learning approach is evaluated in this section with regard to coefficient of determination (R^2), mean absolute error (MAE), and root mean squared error (RMSE). These performance metrics were computed on the training and validation datasets at each cross-validation round, the mean and standard deviation values of which are shown and compared against the AASHTO calculations in Table 3. It should be noted that the prescribed design limits were taken into account while estimating the AASHTO calculations. Here, NAMs-Train, NAMs-Val, and NAMs-Test denote the performance metrics produced by the NAMs on the training, validation, and held-out test datasets, respectively. On the other hand, AASHTO-Train, AASHTO-Val, and AASHTO-Test refer to the same metrics determined by applying the AASHTO provisions to the same training, validation, and test sets used by the NAMs.

In the case of the NAMs, the mean performance metrics on the validation sets are almost on par with those on the training sets. This implies that the model did not overfit during training. It was observed that, with regard to mean R^2, the predictions of the NAMs on the validation sets are about 36.7% more accurate than those of the AASHTO LRFD Bridge Design Specifications. In the same vein, the MAE and RMSE values produced by the NAMs are considerably lower than those of the AASHTO calculations. Moreover, the standard deviation values on the validation sets produced by the NAMs are relatively lower than those by the AASHTO calculations. This indicates that the NAMs predictions are not only more accurate, but also more robust than the AASHTO provisions. Additionally, an ensemble of the ten models obtained from the cross-validation was used to evaluate the performance on the held-out test dataset. It was observed that the NAMs produce an R^2 of 0.77 on the test set, which is 28.3% higher than the corresponding AASHTO value. The same pattern was observed with regard to MAE and RMSE, as well. On the whole, the results presented in Table 3 indicate that the proposed NAMs can serve as a more accurate and robust alternative to the existing AASHTO LRFD shear friction design provisions.

The shape functions obtained from various cross-validation rounds were averaged to obtain the final shape functions, as shown in Figure 3. The bias terms were also combined following the same procedure to produce the final β, which was evaluated as -0.12. The shape functions are also tabulated to enable straightforward reading and interpolation given the normalized input parameters (Table 4).

The proposed LID scheme can be illustrated with the help of an example. Consider specimen 5.5 from Hofbeck et al. (*20*), which had a monolithic interface, 254 mm long and 127 mm wide. The compressive strength of the concrete was 17.2 MPa. The shear reinforcement comprised ten 9.5 mm diameter reinforcing bars with a yield strength of 350 MPa, oriented perpendicular to the shear plane. No normal stress was applied to the shear interface. Let $x = [1, 254, 127, 4.14, 7.72, 90, 0]$ be a set of input parameters characterizing this shear interface, determined by Equations 6 to 12. The objective is to find the corresponding nominal interfacial shear stress. Normalization of the parameters as per Equation 2 produces $\bar{x} = [0, 0.13, 0.05, 0.04, 0.51, 0.67, 0.21]$. Now, for $\bar{x}_1 = 0, f_1(\bar{x}_1)$ can be read from the lookup table (Table 3) to be 0.46. For $\bar{x}_2 = 0.13$, the two nearest neighbors in the lookup table are $u = 0.12$ and $v = 0.14$. Accordingly, $f_2(u) = 0.35$ and $f_2(v) = 0.79$. $f_2(\bar{x}_2)$ can be obtained by a linear interpolation as follows.

$$f_2(\bar{x}_2) = f_2(u) + (f_2(v) - f_2(u)) \times \frac{\bar{x}_2 - u}{v - u} \qquad (13)$$

Equation 13 yields $f_2(\bar{x}_2) = 0.57$. In the same manner, $f_3(\bar{x}_3), f_4(\bar{x}_4), f_5(\bar{x}_5), f_6(\bar{x}_6)$ and $f_7(\bar{x}_7)$ can be estimated as 0.11, -0.98, 4.15, 0.50, and 2.12, respectively. Adding these shape function values according to Equation 1

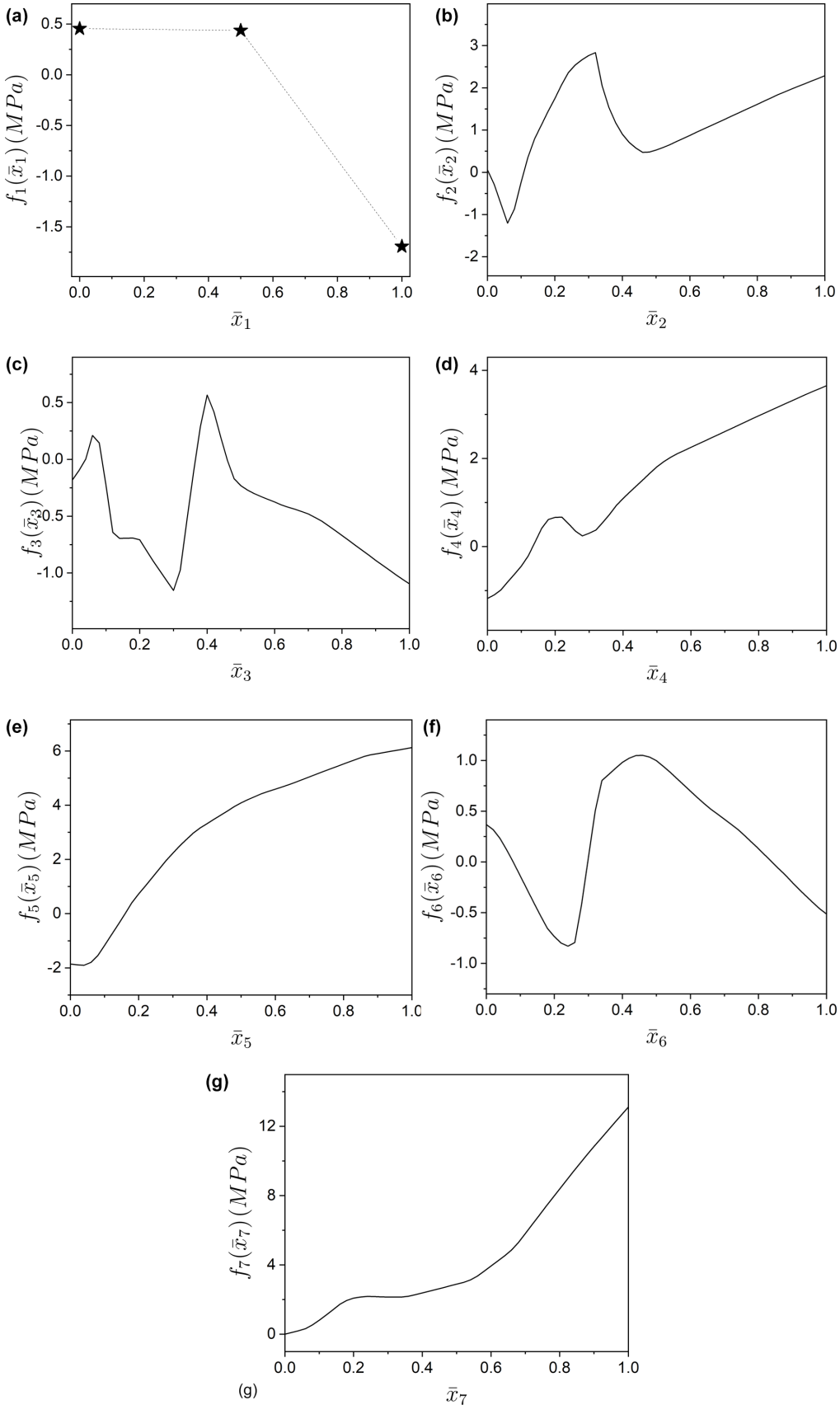

Figure 3. Parameter-specific shape functions: The subfigures (*a*) to (*g*) show the shape functions that correspond to parameters x_1 to x_7.

Table 4. Shape Function Values (in MPa)

$\bar{x}$	$f_1(\bar{x}_1)$	$f_2(\bar{x}_2)$	$f_3(\bar{x}_3)$	$f_4(\bar{x}_4)$	$f_5(\bar{x}_5)$	$f_6(\bar{x}_6)$	$f_7(\bar{x}_7)$
0.00	0.46	0.06	−0.18	−1.18	−1.86	0.37	0.00
0.02		-0.29	−0.10	−1.10	−1.88	0.32	0.10
0.04		−0.74	0.00	−0.98	−1.90	0.23	0.20
0.06		−1.20	0.21	−0.80	−1.80	0.12	0.32
0.08		−0.87	0.14	−0.63	−1.55	−0.01	0.54
0.10		−0.23	−0.23	−0.44	−1.18	−0.14	0.81
0.12		0.35	−0.64	−0.22	−0.79	−0.27	1.11
0.14		0.79	−0.70	0.09	−0.40	−0.41	1.42
0.16		1.12	−0.69	0.42	0.00	−0.53	1.73
0.18		1.44	−0.69	0.62	0.40	−0.65	1.95
0.20		1.75	−0.71	0.66	0.73	−0.73	2.09
0.22		2.07	−0.80	0.67	1.03	−0.80	2.14
0.24		2.36	−0.89	0.51	1.33	−0.83	2.18
0.26		2.54	−0.98	0.35	1.65	−0.79	2.17
0.28		2.66	−1.07	0.24	1.96	−0.42	2.16
0.30		2.77	−1.15	0.30	2.23	0.04	2.15
0.32		2.83	−0.98	0.38	2.50	0.50	2.15
0.34		2.05	−0.54	0.54	2.74	0.80	2.15
0.36		1.54	−0.11	0.73	2.97	0.86	2.19
0.38		1.18	0.29	0.93	3.16	0.92	2.28
0.40		0.90	0.57	1.09	3.32	0.98	2.38
0.42		0.71	0.42	1.24	3.48	1.02	2.48
0.44		0.57	0.20	1.38	3.63	1.05	2.58
0.46		0.47	−0.01	1.53	3.79	1.05	2.68
0.48		0.48	−0.17	1.67	3.95	1.03	2.79
0.50	0.46	0.53	−0.23	1.81	4.09	1.00	2.89
0.52		0.59	−0.27	1.93	4.20	0.94	2.99
0.54		0.65	−0.30	2.02	4.32	0.88	3.13
0.56		0.73	−0.33	2.11	4.43	0.82	3.35
0.58		0.80	−0.35	2.18	4.51	0.76	3.64
0.60		0.87	−0.38	2.25	4.59	0.70	3.94
0.62		0.95	−0.40	2.32	4.67	0.64	4.23
0.64		1.02	−0.42	2.40	4.76	0.58	4.53
0.66		1.10	−0.44	2.47	4.85	0.52	4.86
0.68		1.17	−0.46	2.54	4.95	0.47	5.29
0.70		1.24	−0.48	2.61	5.05	0.42	5.81
0.72		1.32	−0.51	2.68	5.14	0.37	6.33
0.74		1.39	−0.54	2.75	5.24	0.32	6.85
0.76		1.46	−0.58	2.83	5.33	0.26	7.37
0.78		1.54	−0.63	2.90	5.43	0.19	7.88
0.80		1.61	−0.67	2.97	5.52	0.13	8.38
0.82		1.68	−0.71	3.04	5.62	0.06	8.89
0.84		1.76	−0.76	3.11	5.71	0.00	9.39
0.86		1.83	−0.80	3.18	5.80	−0.07	9.88
0.88		1.90	−0.84	3.25	5.86	−0.13	10.37
0.90		1.97	−0.89	3.32	5.90	−0.20	10.83
0.92		2.03	−0.93	3.39	5.95	−0.27	11.29
0.94		2.09	−0.97	3.46	5.99	−0.34	11.75
0.96		2.16	−1.02	3.52	6.04	−0.40	12.21
0.98		2.22	−1.06	3.59	6.08	−0.46	12.66
1.00	−1.69	2.29	−1.10	3.65	6.13	−0.51	13.12

results in $y = 6.79$ MPa. This predicted value of the interfacial shear strength closely tallies with the observed value of 6.96 MPa (*20*). On the other hand, the AASHTO LRFD Bridge Design Specifications (Equation 3) predict an interfacial shear stress of 4.29 MPa for this specimen, which is far less accurate than the LID prediction.

In this way, the interfacial shear strength values were predicted for all the specimens using Table 4. The predicted values are plotted against the test results in Figure 4.

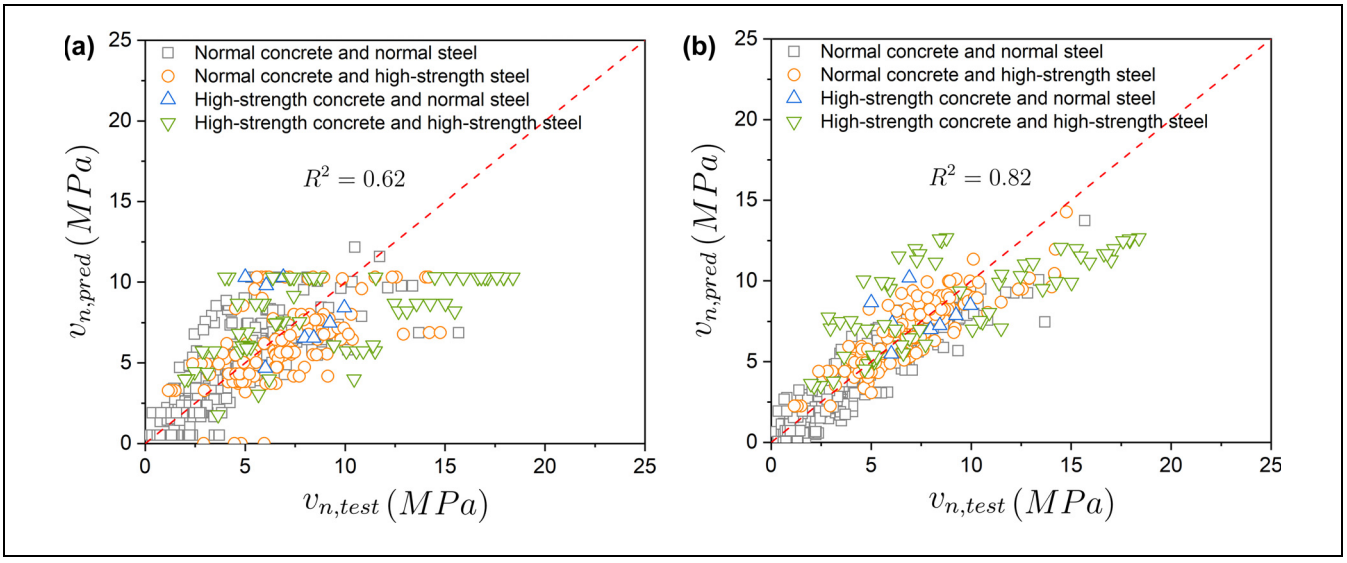

Figure 4. Prediction accuracy of the existing and proposed design schemes; $v_{n,\,test}$ and $v_{n,\,pred}$ denote the experimental and predicted values of interfacial shear strength, respectively. (*a*) AASHTO LRFD and (*b*) LID Scheme.
Note: LID = learning-informed design.

Note that $v_{n,test}$ and $v_{n,pred}$ denote the experimental and predicted values of nominal interfacial shear stress (in MPa), respectively. The proposed LID scheme and the AASHTO calculations produce an R^2 of 0.82 and 0.62, respectively. In other words, the proposed approach is 32.3% more accurate than the AASHTO LRFD Bridge Design Specifications. It is further observed that the relative superiority of the proposed LID scheme cuts across normal and high-strength materials (Figure 4). Concrete specimens having compressive strength greater than 60 MPa are designated in this study as high-strength concrete. On the other hand, steel reinforcement having yield strength greater than 420 MPa is identified as high-strength steel. Evidently, the proposed LID scheme can help improve the current design provisions ensuring a safer and more economical design of RC components. However, there are some unconservative predictions, that is, predicted value higher than the experimental value, particularly for specimens with high-strength concrete and high-strength steel. Future studies should aim to reduce the extent of overestimation to address the needs of a conservative design paradigm.

Conclusions

This study proposed a generalized framework for developing a LID scheme to aid in the accurate and interpretable prediction of various structural strength and response parameters. It has been demonstrated through a case study on shear friction at the normalweight concrete-to-concrete interface that the proposed approach results in a new design paradigm that can significantly outperform the existing design specifications. Based on data collected from the literature and seven key parameters identified based on physical insights, the accuracy of the proposed LID approach in predicting the interfacial shear strength was demonstrated to be over 32% higher than that of the existing AASHTO LRFD Bridge Design Specifications. The results of the LID scheme are also more robust and interpretable, as the contribution of each input parameter to the final prediction can be ascertained on an individual basis. With appropriate case-specific modifications, this technique can be extended in the future to many other application areas, including but not limited to the estimation of the residual strength of corroded steel members, the fatigue resistance of welded steel connections, and the capacity of different types of piles in soil. On the downside, the proposed LID scheme does not account for the pairwise interaction effects between different design parameters, which is a scope of further investigation.

Author Contributions

The authors confirm contribution to the paper as follows: study conception and design: Tarutal Ghosh Mondal, Genda Chen; data collection: Nikkolas Edgmond, Lesley Sneed; analysis and interpretation of results: Tarutal Ghosh Mondal; draft manuscript preparation: Tarutal Ghosh Mondal. All authors reviewed the results and approved the final version of the manuscript.

Declaration of Conflicting Interests

The author(s) declared no potential conflicts of interest with respect to the research, authorship, and/or publication of this article.

Funding

The author(s) disclosed receipt of the following financial support for the research, authorship, and/or publication of this article: Financial support to complete this study was provided by the U.S. Department of Transportation, Office of Assistant Secretary for Research and Technology under the auspices of the Mid-America Transportation Center at the University of Nebraska, Lincoln (grant no. 00065573).

ORCID iDs

Tarutal Ghosh Mondal https://orcid.org/0000-0003-2091-7046
Lesley Sneed https://orcid.org/0000-0003-1528-5611

References

1. AASHTO. *LRFD Bridge Design Specifications*. American Association of State Highway and Transportation Officials (AASHTO), Washington, D.C., Standard 9th Edition, 2020.
2. ACI. *Building Code Requirements for Structural Concrete (ACI 318-14) and Commentary (ACI 318R-19)*. American Concrete Institute (ACI), Farmington Hills, MI, Standard, 2019.
3. Barbosa, A. R., D. Trejo, and D. Nielson. Effect of High-Strength Reinforcement Steel on Shear Friction Behavior. *Journal of Bridge Engineering*, Vol. 22, No. 8, 2017, p. 04017038.
4. Kahn, L. F., and A. D. Mitchell. Shear Friction Tests with High-Strength Concrete. *Structural Journal*, Vol. 99, No. 1, 2002, pp. 98–103.
5. Edgmond, N. J., and L. H. Sneed. *Examination of Shear Friction Design Provisions*. Tech. Report. Pre- cast/Prestressed Concrete Institute (PCI), Chicago, IL, 2019, p. 147.
6. Goh, A. T. Back-Propagation Neural Networks for Modeling Complex Systems. *Artificial Intelligence in Engineering*, Vol. 9, No. 3, 1995, pp. 143–151.
7. Hu, X., B. Li, Y. Mo, and O. Alselwi. Progress in Artificial Intelligence-Based Prediction of Concrete Performance. *Journal of Advanced Concrete Technology*, Vol. 19, No. 8, 2021, pp. 924–936.
8. Duan, Z.-H., S.-C. Kou, and C.-S. Poon. Prediction of Compressive Strength of Recycled Aggregate Concrete Using Artificial Neural Networks. *Construction and Building Materials*, Vol. 40, 2013, pp. 1200–1206.
9. Dantas, A. T. A., M. B. Leite, and K. De Jesus Nagahama. Prediction of Compressive Strength of Concrete Containing Construction and Demolition Waste Using Artificial Neural Networks. *Construction and Building Materials*, Vol. 38, 2013, pp. 717–722.
10. Asteris, P. G., D. J. Armaghani, G. D. Hatzigeorgiou, C. G. Karayannis, and K. Pilakoutas. Predicting the Shear Strength of Reinforced Concrete Beams Using Artificial Neural Networks. *Computers and Concrete, An International Journal*, Vol. 24, No. 5, 2019, pp. 469–488.
11. Bashir, R., and A. Ashour. Neural Network Modelling for Shear Strength of Concrete Members Reinforced with FRP Bars. *Composites Part B: Engineering*, Vol. 43, No. 8, 2012, pp. 3198–3207.
12. Demir, F. Prediction of Elastic Modulus of Normal and High Strength Concrete by Artificial Neural Networks. *Construction and Building Materials*, Vol. 22, No. 7, 2008, pp. 1428–1435.
13. Chen, D., and W. Ye. Generalized Gloves of Neural Additive Models: Pursuing Transparent and Accurate Machine Learning Models in Finance. *arXiv Preprint arXiv:2209.10082*, 2022.
14. Jo, W., and D. Kim. Neural Additive Models for Nowcasting. *arXiv Preprint arXiv:2205.10020*, 2022.
15. Peroni, M., M. Kurban, S. Y. Yang, Y. S. Kim, H. Y. Kang, and J. H. Song. Extending the Neural Additive Model for Survival Analysis with EHR Data. *arXiv Preprint arXiv:2211.07814*, 2022.
16. Balabaeva, K., and S. Kovalchuk. Neural Additive Models for Explainable Heart Attack Prediction. *Proc., Computational Science–ICCS 2022: 22nd International Conference*, London, June 21–23, 2022, Part III, Springer, Cham, Switzerland, pp. 113–121.
17. Agarwal, R., L. Melnick, N. Frosst, X. Zhang, B. Lengerich, R. Caruana, and G. E. Hinton. Neural Additive Models: Interpretable Machine Learning with Neural Nets. *Advances in Neural Information Processing Systems*, Vol. 34, 2021, pp. 4699–4711.
18. Xu, S., Z. Bu, P. Chaudhari, and I. J. Barnett. Sparse Neural Additive Model: Interpretable Deep Learning with Feature Selection via Group Sparsity. *arXiv Preprint arXiv:2202.12482*, 2022.
19. Kingma, D. P., and J. Ba. Adam: A Method for Stochastic Optimization. *arXiv Preprint arXiv:1412.6980*, 2014.
20. Hofbeck, J. A., I. O. Ibrahim, and A. H. Mattock. Shear Transfer in Reinforced Concrete. *Journal Proceedings*, Vol. 66, No. 2, 1969, pp. 119–128.